THE JOURNAL OF PHYSICAL CHEMISTRY Letters

Letter

Cite This: J. Phys. Chem. Lett. 2019, 10, 5428−5433

pubs.acs.org/JPCL

Single-Molecule Force Spectroscopy Reveals that Iron−Ligand Bonds Modulate Proteins in Different Modes

Guodong Yuan, Huaxing Liu, Qun Ma, Xi Li, Jingyuan Nie, Jinglin Zuo, and Peng Zheng*

State Key Laboratory of Coordination Chemistry, School of Chemistry and Chemical Engineering, Nanjing University, Nanjing, Jiangsu 210023, People's Republic of China

Supporting Information

ABSTRACT: The iron−amino acid interactions Fe−O(Glu/Asp), Fe−N(His), and Fe−S(Cys) are the three major iron−ligand bonds in proteins. To compare their properties in proteins, we used atomic force microscopy (AFM)-based single-molecule force spectroscopy to investigate a superoxide reductase (Fe(III)-SOR) with all three types of bonds forming an $Fe(His)_4CysGlu$ center. We first found that Apo-SOR without bound iron showed multiple unfolding pathways only from the β-barrel core. Then, using Holo-SOR with a ferric ion, we found that a single Fe−O(Glu) bond can tightly connect the flexible N-terminal fragment to the β-barrel and stabilize the whole protein, showing a complete protein unfolding scenario, while the single Fe−N(His) bond was weak and unable to provide such a stabilization. Moreover, when multiple Fe−N bonds are present, a similar stabilization effect can be achieved. Our results showed that the iron−ligand bond modulates protein structure and stability in different modes at the single-bond level.

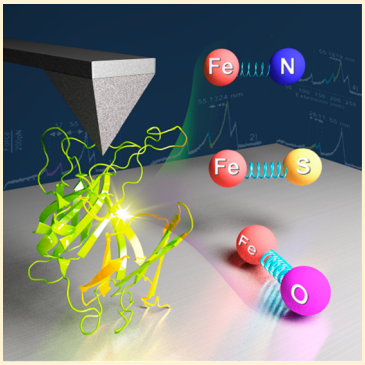

Transition metal ions are ubiquitous and play essential roles in biology.[1−3] As the most abundant trace metal in the human body, iron is one of the most crucial chemical ingredients in life. Iron binds to proteins, and iron-containing proteins are indispensable for diverse biological processes such as oxygen storage and many critical, enzyme-catalyzed reactions.[4,5] Iron binds to proteins mainly through the formation of three different metal−ligand coordination bonds, namely, to the carboxylate oxygen in glutamic/aspartic acid to form an Fe−O(Glu) bond, to the imidazole nitrogen in histidine to form an Fe−N(His) bond, and to the sulfur in cysteine to form an Fe−S(Cys) bond. Moreover, these bonds are usually present in the different types of proteins at different frequencies. Consequently, the comparison of the properties of these three different Fe−ligand bonds and their corresponding modulation modes for proteins provides valuable insight into the role of iron in protein structure and stability.

To accurately characterize their contributions in one molecule, we chose AFM-based single-molecule force spectroscopy (SMFS) to study the iron binding effect in an iron-containing protein superoxide reductase (SOR), which contains all three types of bonds (Fe−N(His), Fe−O(Glu), and Fe−S(Cys) bonds). SMFS, including single-molecule AFM and optical and magnetic tweezers, is a powerful technique that can mechanically manipulate single biomacromolecules.[6−15] Among these techniques, single-molecule AFM has been widely applied to study protein (un)folding processes, protein−ligand interactions, and even chemical bonds because of its high force range.[16−27] It is also used to study the metal−ligand coordination bonds in both inorganic and protein systems.[28−32] Thus, we used AFM here to study the unfolding process of Fe(III)-SOR and to directly quantify the Fe−ligand bond strength.

Fe(III)-SOR is a blue-colored protein whose biochemical and spectroscopic properties have been extensively characterized.[33,34] SOR is a defense protein against reactive oxygen in anaerobic microbes that catalyzes the conversion of superoxide to hydrogen peroxide. The X-ray crystallography structure of the ferric form of SOR shows that the protein adopts an immunoglobulin (Ig)-like β-barrel fold core with seven β strands A−G and an N-terminal flexible fragment (N-frag) from residues 1−18. SOR contains a mononuclear, nonheme iron center that is coordinated by four imidazole nitrogens (His16, His41, His47, and His114, H16,41,47,114), one cysteinyl sulfur (Cys111, C111), and one glutamic carboxylate (Glu14, E14, COO^-), forming a six-coordinate octahedral iron center, $Fe(His)_4CysGlu$ (Figure 1A).[33−35] Here, the glutamic acid is depronated under neutral pH and coordinates to the ferric ion as a monodentate ligand. In the Fe(III)-bound form (named the Holo-form), the Fe−O(Glu14) bond and the Fe−N(His16) bond connect the flexible N-terminal fragment to the β-barrel core. Interestingly, besides the six-coordinated metal center, the X-ray crystallographic structure shows that a half-quantity of Holo-SOR adopts a five-coordinate iron site lacking the Fe−O bond, and the biological meaning is still unclear. Nevertheless, two types of iron centers exist in the Holo-SOR as the N-terminal fragment is connected to the iron center with both an Fe−O(Glu14) bond and an Fe−N(His16) bond or with only one Fe−N(His16) bond. Consequently, the

Received: June 1, 2019
Accepted: August 21, 2019
Published: August 21, 2019

DOI: 10.1021/acs.jpclett.9b01573
J. Phys. Chem. Lett. 2019, 10, 5428−5433

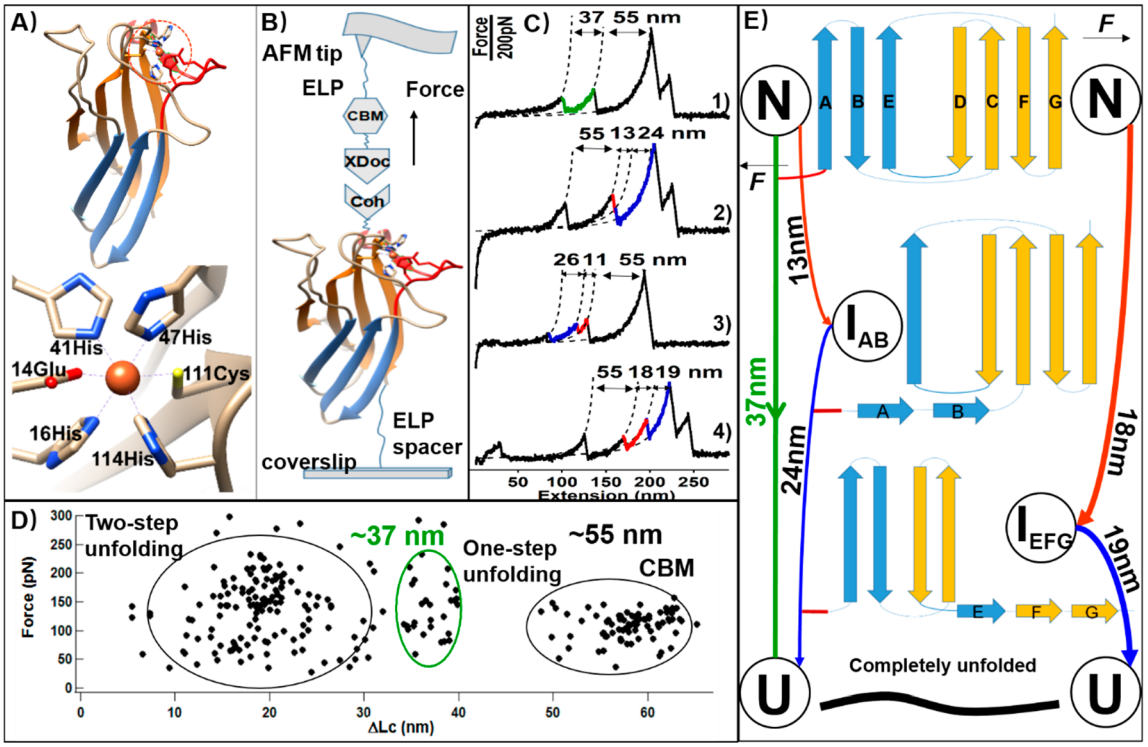

Figure 1. (A) SOR is an iron-containing protein with an N-terminal fragment and a β-barrel core (PDB code: 1DO6). The iron is coordinated by six residues forming an $Fe(His)_4CysGlu$ center. (B) Setup of an AFM experiment displaying how the covalently attached SOR is unfolded. (C) Representative force−extension curves of the Apo-SOR showing multiple unfolding pathways. The single force peak with ΔLc of 37 nm (curve 1) corresponds to the one-step unfolding of the Ig-fold β-barrel, and the other three types with a cumulative ΔLc of 37 nm were from the two-step unfolding of the barrel (curve 2−4). (D) Scatter plot between the unfolding force and ΔLc showing these unfolding pathways. The peak with ΔLc of 55 nm was from the marker protein cellulose-binding module (CBM). (E) Cartoon showing the mechanism of the three major unfolding pathways of Apo-SOR. The one green line indicates a one-step unfolding scenario, while the stepwise lines with two colors indicate two-step unfolding with a partially unfolded intermediate shown. The percentage of each pathway is represented by the width of the line.

three primary iron−ligand bonds in the iron-containing protein, including one Fe−O bond, four Fe−N bonds, and one Fe−S bond, are present in the Holo-SOR. This structure thus fulfills our purpose of studying the modulation effect of the different Fe−ligand bonds in one protein molecule.

To ensure an accurate measurement of the Fe−ligand bond in Fe-SOR, a fused protein construct cohesin-SOR-Asn-Gly-Leu (Coh-SOR-NGL) with a molecular weight of ∼43 kDa was built for single-molecule AFM experiments (Figure S1). The C-terminal fragment NGL enables covalent attachment of SOR on the functional glass surface, and cohesin leads to a specific pickup of SOR by the AFM tip (Figure 1B).[36−40] Cohesin forms a specific protein−protein interaction with dockerin (Doc), and the C-terminal NGL residues react with the N-terminal GL residues (Gly-Leu), forming a covalent NGL peptide linkage. This configuration led to a completely site-specifically conjugated construct from the AFM tip to the glass coverslip, in which SOR was present in between. By moving the AFM tip away vertically, the SOR protein was stretched, leading to the unfolding of SOR and the rupture of Fe−ligand bonds.

To distinguish the iron binding effect of SOR from the protein secondary structure, we first studied the SOR without iron binding (named Apo-SOR). The Apo-SOR sample was prepared, and its purity was confirmed by inductively coupled plasma mass spectrometry (ICP-MS), showing less than 10% residual iron (SI).[33,34] When stretched by single-molecule AFM, the Apo-SOR showed a characteristic sawtooth-like force−extension curve in which each force peak corresponded to the unfolding event of a protein or a particular protein fragment (Figure 1C). The force−extension curves were first analyzed by fitting the polymer elasticity using the worm-like chain (WLC) model, and the specific contour length increment (ΔLc) for each force peak was obtained.[41] ΔLc describes how long the protein backbone extends after protein unfolding, which is a characteristic of a particularly stable protein or a fragment after unfolding/extension. For example, the largest ΔLc value of the Apo-SOR unfolding peak is 37 nm (37.1 ± 1.9 nm, average length and standard deviation, Figure 1C, curve 1), attributed to the unfolding of the seven-stranded β-barrel structure of SOR from residues 19 to 123 because 105 amino acids are extended after the β-barrel unfolding (theoretical ΔLc: 0.365 × 105 − 1.5 = 36.5 nm; 1.5 nm is the original distance between residues 19 and 123, which needs to be subtracted, Figure S2). The average unfolding force and standard deviation for this scenario was 146 ± 58 pN (n = 30), which is comparable to that of most stable Ig-like folding proteins.[42−45] Notably, an unfolding event of the unstructured N-terminal fragment from residues 1 to 18 outside of the β-barrel structure was not detected. Otherwise, a force peak with the ΔLc value of 4.5 nm should be observed (0.365 × 18 − 2.1 = 4.5 nm, Figure S2). This fragment was labile, with an unfolding force below the detection limit of AFM, and it unfolds first before the β-barrel core structure. More details for using ΔLc to explain the protein unfolding scenario and mechanism can be found in the SI.

DOI: 10.1021/acs.jpclett.9b01573
J. Phys. Chem. Lett. 2019, 10, 5428−5433

Table 1. Data Summary for Each SOR Unfolding Scenario

state	mode	ΔLc (nm)	*F* (pN)	%	protein and Fe−L bonds broken
Apo	37	37.1 ± 1.9	146 ± 58	31	ABCDEFG (A-G)
	18 + 19	18; 19	154 ± 56	44	EFG (I_{EFG}); ABCD (A-D)
	13 + 24	13.3 ± 1.5	155 ± 83	16	AB (I_{AB})
		25.1 ± 1.8	132 ± 65		CDEFG (C-G)
	26 + 11	27.4 ± 1.2	113 ± 66	9	ABCDE
		11.2 ± 0.9	89 ± 45		FG
Holo-6	42	41.6 ± 1.6	127 ± 54	33	A-G + **E14** + H16,41,47,114 + C111
	14 + 28	13.9 ± 2.3	109 ± 50	54	FG + C111 + H114 (I_{FG})
		28.7 ± 2.0	210 ± 89		ABCDE + **E14** + H16,41,47
	19 + 23	20.0 ± 1.0	219 ± 48	13	AB + **E14** + H16,41
		22.7 ± 1.0	178 ± 51		C-G + H47,114 + C111
Holo-5	37	37.2 ± 1.4	149 ± 54	60	A-G + H16,41,47,114 + C111
	18 + 19	18; 19	209 ± 56	40	EFG + C111 + H114; A-D + H16,41,47

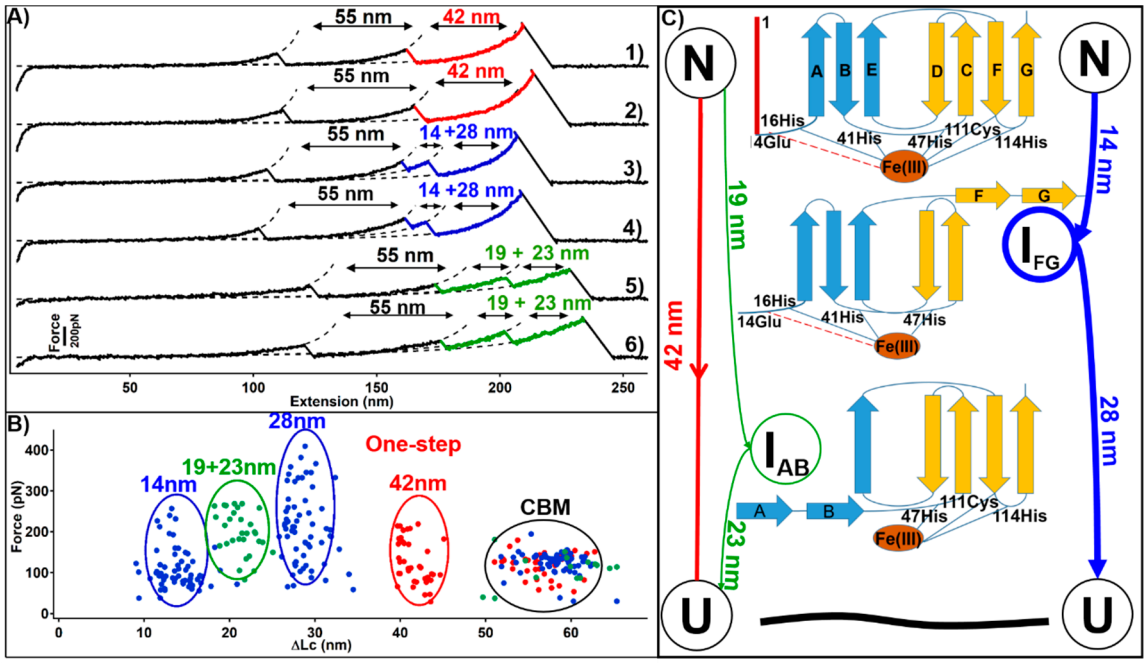

Figure 2. (A) Representative curves of Holo-SOR with a six-coordinate iron center including an Fe−O bond showed a single force peak with ΔLc of 42 nm (curves 1 and 2, colored in red) and the stepwise force peaks with a cumulative ΔLc value of 42 nm (curves 3−6). (B) The scatter map showed all of these pathways. (C) The schematics indicate the stepwise unfolding scenarios with a combination of ΔLc of 14 + 28 and 19 + 23 nm.

In addition to this one-step unfolding event, several two-step unfolding events with two stepwise peaks were observed (Figure 1C, curves 2−4). The sum of their ΔLc values was also 37 nm, which agrees well with the value of the unfolding of the entire β-barrel structure revealed above. Thus, these events describe the stepwise unfolding patterns of Apo-SOR. For example, the first peak, with a ΔLc value of 13 nm, was attributed to unfolding of the β strands A and B (residue 19−48, theoretical ΔLc = 0.365 × 30 − 1.2 = 9.8 nm), and the second peak, with a ΔLc value of 24 nm, was attributed to strands C-G (residue 50−123, theoretical ΔLc = 0.365 × 74 − 2.3 = 24.7 nm, n = 15). In addition, another stepwise unfolding scenario with two force peaks with ΔLc values of 18 nm was attributed to unfolding of the β strands E-G (residue 71−123) and β strands A-D (residue 19−70, n = 42). Finally, a stepwise unfolding scenario with a ΔLc value of 26 + 11 nm (n = 9) was also detected. Such multiple stepwise unfolding events indicate that the β-barrel structure in Apo-SOR is dynamic as the most stable single-domain protein unfolds in one defined pathway under mechanical manipulation. Detailed results such as the unfolding mode and force are summarized in Table 1.

Next, we stretched the Holo-form SOR to study the effect of iron binding to the protein. Compared with the Apo-SOR, the Holo-SOR showed an unfolding event with a larger ΔLc of 42 nm (41.6 ± 1.6 nm, n = 39, 33%, Figure 2A,B). This value agrees well with the complete unfolding of SOR from the first residue to the last (124th) residue (0.365 × 124 − 2.6 = 42.6 nm), including the previously undetected N-terminal fragment in the Apo-form. The average force was 127 ± 54 pN.

Moreover, two major stepwise unfolding scenarios were observed with a cumulative ΔLc value of 42 nm. The ΔLc combination of 14 + 28 nm (n = 63, 54%) and 19 + 23 nm (n = 15, 13%) was observed (Figure 2A). Both scenarios with larger ΔLc values are attributed to incorporation of the N-terminal fragment bound by the Fe−O(Glu) bond. The 14 + 28 nm scenario is similar to the previous 11 + 26 nm scenario observed for the Apo-form. The first peak, with a ΔLc value of 14 nm, was attributed to unfolding of the N-terminal fragment

DOI: 10.1021/acs.jpclett.9b01573
J. Phys. Chem. Lett. 2019, 10, 5428−5433

(4.5 nm, residues 1−14) plus β strands F-G (8.0 nm, residue 100−123), and the second peak, with a ΔLc value of 28 nm, was attributed to strands A-E (residue 15−99). Similarly, a value of 19 nm was from the unfolding of the N-terminal fragment together with β strands A and B (residue 1−47), and the second peak, with a ΔLc value of 23 nm, was attributed to strands C-G (residue 48−123). Both mechanisms are shown in Figure 2C. The unfolding event of Holo-SOR with a larger ΔLc value of 42 nm indicated that the Fe−O bond connects the N-terminal peptide fragment to the β-barrel core and stabilizes the protein structure and stability.

On the basis of the structure determined by X-ray crystallography, a half-quantity of the Holo-SOR protein lacks the Fe−O(Glu) bond and instead contains a five-coordinate center, $Fe(His)_4Cys$. Indeed, a one-step unfolding event of Holo-SOR with a ΔLc of 37 nm (n = 85, 60%), previously observed in Apo-SOR, was also observed here. The two-step unfolding scenario with a summed ΔLc value of 37 nm was observed. However, only one type of the two-step unfolding pattern with a ΔLc combination of 18 + 19 nm was observed (Figure 3A, curves 3 and 4, n = 56, 40%). Thus, these

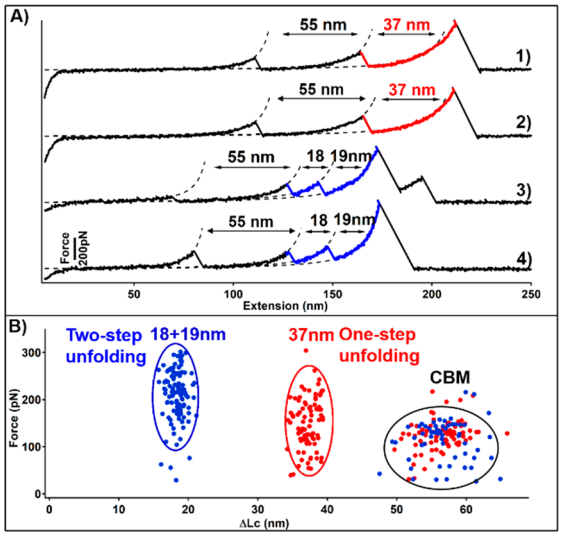

Figure 3. (A) Representative curves of Holo-SOR with a five-coordinate iron center without an Fe−O bond showing a single force peak with ΔLc of 37 nm (curves 1 and 2) as well as one type of stepwise force peak with a ΔLc combination of 18 + 19 nm (curves 3 and 4). (B) The scatter plot showed a one-step pathway and one type of two-step unfolding pathway.

events were most likely from the five-coordinate $Fe(His)_4Cys$ metal site and suggest that iron binding still stabilizes the β-barrel core structure. Here, the Fe−N (His 16) bond was still formed in this five-coordinate center. However, the unfolding of the N-terminal fragment was not observed, indicating that the single Fe−N(His) bond does not provide such stabilization.

In this Letter, we studied the unfolding process of an iron-containing protein, SOR, in its Apo-form, a six-coordinate iron center Holo-form, and a five-coordinate form. Holo-SOR contains the three major different iron−ligand bond types for iron-containing proteins. First, a complete unfolding event of the entire SOR containing a six-coordinate iron center with a ΔLc of 42 nm was observed, while the Apo-form seldomly showed such an event. This finding indicates that the formation of a single Fe−O(Glu) bond connects the N-terminal peptide fragment to the β-barrel core and stabilizes this structure to a large extent. Moreover, it suggested that the iron binding could modulate the protein stability and unfolding pattern by a single Fe−O bond. Indeed, the presence of a single Fe−O bond in the protein metal center as a stable site is widely observed.[4,46] Interestingly, a five-coordinate iron center is also present in the SOR proteins. Here, the Fe−O(Glu) bond is missing, but the Fe−N(His16) bond is still formed and connects the N-terminal fragment to the β-barrel core. However, the complete unfolding event is absent, similar to the Apo-form. For comparison, the unfolding force of SOR involving the Fe−O bond for single-step unfolding is 127 pN, while the force for the single Fe−N(His16) bond is undetected (<15 pN). This result confirmed the importance of the single Fe−O bond for protein stabilization as well as indicating that the single Fe−N bond was not stable enough to hold the N-terminal fragment tightly to the β-barrel core.

Moreover, the unfolding forces of Holo-SOR including the Fe−O bond were higher than those from Apo-SOR. The stepwise unfolding force for Holo-SOR is ∼220 pN compared with ∼140 pN for Apo-SOR. Indeed, previous studies showed that the substitution of Fe−S bonds by an unnatural Fe−N bond reduced the stability of the iron−sulfur center in rubredoxin (<15 pN).[47] Here, it is further proved in a natural protein. This strong Fe−O bond provides insight into why Fe−O bonds are usually present in proteins with a high iron binding affinity, such as transferrin and ferritin. These proteins transfer and store iron, utilizing the catechol as the basic unit to chelate iron. Comparing the nature of the two coordination bonds, additional ionic interaction is present between the ferric ion and COO^- for the Fe−O bond, while no ionic character is present for imidazole nitrogen under neutral pH. Thus, this additional ionic interaction may explain why the strength of Fe−O is significantly stronger than that of Fe−N.

It is noted that the Holo-SOR without the Fe−O bond is also more stable than the Apo-SOR. The forces from stepwise unfolding are ∼210 pN, compared with 130 pN from the Apo-SOR. Moreover, a lesser stepwise unfolding scenario is observed in the Holo-SOR than that of Apo-SOR. Thus, the formation of multiple Fe−N bonds stabilizes the proteins to a certain extent. Indeed, Fe−N bonds are present more frequently as multiple bonds for iron-containing proteins. Finally, Fe−S bonds in proteins have been extensively characterized previously by single-molecule AFM using the small iron−sulfur protein rubredoxin, showing a rupture force of 200 pN, indicative of a stable metal−ligand bond.[47] Here, our results are consistent with these findings and provide a comparison between Fe−O(Glu) and Fe−N(His) bonds for the first time.

Metals are ubiquitous in proteins, and more than 30% of proteins contain metals and are termed metalloprotein. Metals play both important functional and structural roles in proteins. To date, the strengths of several metal sites in metalloprotein systems have been measured using single-molecule AFM, such as the FeS_4 center in rubredoxin,[47] the Fe_2S_2 in the ferredoxin,[28] the $Zn(Cys)_4$ site in the zinc finger protein DnaJ,[48] the $Cu(His)_2CysMet$ site in the cupredoxin,[30] and the Au−S site in GolB.[49] All of these metal sites showed a measurable rupture force, ranging from 50 to 300 pN. Thus, most metal sites forming between transitional metals, such as Fe, Zn, and Cu, and the ligand from protein residues, such as S,

DOI: 10.1021/acs.jpclett.9b01573
J. Phys. Chem. Lett. 2019, 10, 5428−5433

N, and O, are mechanostable and can be an independent unfolding barrier for protein systems.

In conclusion, by using iron-containing protein SOR with an $Fe(His)_4CysGlu$ center, we discovered that the three different types of Fe−ligand bonds modulate the protein structure and stability in different modes. A single Fe−O(Glu) bond is sufficient to stabilize the protein structure, while multiple Fe−N(His) bonds are needed for a similar effect.

MATERIALS AND METHODS

The gene encoding for the protein was ordered from Genscript Inc.: type III cohesin-dockerin X domain complex from *Ruminococcus flavefacience* (Coh-XDoc), the cellulose-binding module (CBM), elastin-like polypeptides (ELPs), and SOR from *Pyrococcus furiosus* (SOR).[33,40] The peptide tags GL and NGL were added by regular PCR if needed. The protein overexpression was conducted using *E. coli.* BL21(DE3) cells. An established protocol was used for protein expression and purification and Apo-SOR preparation, described in details in the SI.[33,50]

AFM experiments were performed using a Nanowizard4 (JPK) atomic force microscope. The MLCT cantilever was calibrated in the AFM buffer solution using the equipartition theorem, and a spring constant of 50 $pN{\cdot}nm^{-1}$ was usually obtained. The cantilevers used in the single-molecule AFM experiments were silicon-based materials (MLCT, Bruker). The glass coverslip was also a silicon-based material. Thus, the classic method was used to functionalize the AFM tip and coverslip and immobilize the polyprotein.[36,51] All AFM experiments were performed in Tris buffer at pH 7.4. Protein Coh-SOR-NGL in 50 μL solution (0.5 mg/mL containing 100 nM OaAEP, pH 7.4) was dropped onto the GL-modified coverslip at 25 °C for 30 min. Under this condition, the iron in SOR was the ferric form. Then, the AFM experiment was performed at a constant pulling speed of 400 $nm{\cdot}s^{-1}$. In the experiment, fused cohesin forms a specific protein−protein interaction with the dockerin (Doc) functionalized on the AFM tip. The Doc/Coh interaction is of high rupture force of ~500 pN, which ensures that all of the proteins are unfolded.[36,40] Thus, all of the force−extension curves that we selected for analysis were of this high rupture force.

A more detailed explanation of different unfolding pathways of Apo-SOR is shown in Figure S2. The different unfolding force peaks from Apo-SOR were assigned to specific protein fragments based on the characteristic contour length increment (ΔLc).

ASSOCIATED CONTENT

Supporting Information

The Supporting Information is available free of charge on the ACS Publications website at DOI: 10.1021/acs.jpclett.9b01573.

Materials and methods, protein sequences, SDS-PAGE gels of SOR, and unfolding schematics of Apo-SOR (PDF)

AUTHOR INFORMATION

Corresponding Author

*E-mail: pengz@nju.edu.cn.

ORCID

Jinglin Zuo: 0000-0003-1219-8926

Peng Zheng: 0000-0003-4792-6364

Author Contributions

P.Z. and G.D.Y. designed the research, G.D.Y. and Q.M. performed the experiments, G.D.Y. H.X.L., and Q.M. analyzed the data and prepared the figures, and P.Z., J.L.Z., and G.D.Y. wrote the manuscript.

Funding

This work was supported by the National Natural Science Foundation of China (Grant No. 21771103, 21977047), the Natural Science Foundation of Jiangsu Province (Grant No. BK20160639), and Shuangchuang Program of Jiangsu Province.

Notes

The authors declare no competing financial interest.

REFERENCES

(1) Waldron, K. J.; Rutherford, J. C.; Ford, D.; Robinson, N. J. Metalloproteins and metal sensing. *Nature* **2009**, *460* (7257), 823−830.

(2) Holm, R. H.; Kennepohl, P.; Solomon, E. I. Structural and Functional Aspects of Metal Sites in Biology. *Chem. Rev.* **1996**, *96* (7), 2239−2314.

(3) Winkler, J. R.; WittungStafshede, P.; Leckner, J.; Malmstrom, B. G.; Gray, H. B. Effects of folding on metalloprotein active sites. *Proc. Natl. Acad. Sci. U. S. A.* **1997**, *94* (9), 4246−4249.

(4) Garcia, J. S.; Magalhães, C. S. d.; Arruda, M. A. Z. Trends in metal-binding and metalloprotein analysis. *Talanta* **2006**, *69* (1), 1−15.

(5) Liu, J.; Chakraborty, S.; Hosseinzadeh, P.; Yu, Y.; Tian, S.; Petrik, I.; Bhagi, A.; Lu, Y. Metalloproteins containing cytochrome, iron-sulfur, or copper redox centers. *Chem. Rev.* **2014**, *114* (8), 4366−469.

(6) Dufrêne, Y. F.; Evans, E.; Engel, A.; Helenius, J.; Gaub, H. E.; Müller, D. J. Five challenges to bringing single-molecule force spectroscopy into living cells. *Nat. Methods* **2011**, *8*, 123.

(7) Woodside, M. T.; Block, S. M. Reconstructing Folding Energy Landscapes by Single-Molecule Force Spectroscopy. *Annu. Rev. Biophys.* **2014**, *43*, 19−39.

(8) Carrion-Vazquez, M.; Oberhauser, A. F.; Fowler, S. B.; Marszalek, P. E.; Broedel, S. E.; Clarke, J.; Fernandez, J. M. Mechanical and chemical unfolding of a single protein: A comparison. *Proc. Natl. Acad. Sci. U. S. A.* **1999**, *96* (7), 3694−3699.

(9) Yu, M.; Le, S.; Efremov, A. K.; Zeng, X.; Bershadsky, A.; Yan, J. Effects of Mechanical Stimuli on Profilin- and Formin-Mediated Actin Polymerization. *Nano Lett.* **2018**, *18* (8), 5239−5247.

(10) Walder, R.; Van Patten, W. J.; Ritchie, D. B.; Montange, R. K.; Miller, T. W.; Woodside, M. T.; Perkins, T. T. High-Precision Single-Molecule Characterization of the Folding of an HIV RNA Hairpin by Atomic Force Microscopy. *Nano Lett.* **2018**, *18* (10), 6318−6325.

(11) Guinn, E. J.; Tian, P.; Shin, M.; Best, R. B.; Marqusee, S. A small single-domain protein folds through the same pathway on and off the ribosome. *Proc. Natl. Acad. Sci. U. S. A.* **2018**, *115* (48), 12206−12211.

(12) Hickman, S. J.; Cooper, R. E. M.; Bellucci, L.; Paci, E.; Brockwell, D. J. Gating of TonB-dependent transporters by substrate-specific forced remodelling. *Nat. Commun.* **2017**, *8*, 14804.

(13) Sen Mojumdar, S.; Scholl, Z. N.; Dee, D. R.; Rouleau, L.; Anand, U.; Garen, C.; Woodside, M. T. Partially native intermediates mediate misfolding of SOD1 in single-molecule folding trajectories. *Nat. Commun.* **2017**, *8* (1), 1881.

(14) Hoffer, N. Q.; Neupane, K.; Pyo, A. G. T.; Woodside, M. T. Measuring the average shape of transition paths during the folding of a single biological molecule. *Proc. Natl. Acad. Sci. U. S. A.* **2019**, *116* (17), 8125−8130.

(15) Berkovich, R.; Fernandez, V. I.; Stirnemann, G.; Valle-Orero, J.; Fernández, J. M. Segmentation and the Entropic Elasticity of Modular Proteins. *J. Phys. Chem. Lett.* **2018**, *9* (16), 4707−4713.

DOI: 10.1021/acs.jpclett.9b01573
J. Phys. Chem. Lett. 2019, 10, 5428−5433

(16) Thoma, J.; Sapra, K. T.; Müller, D. J. Single-Molecule Force Spectroscopy of Transmembrane β-Barrel Proteins. *Annu. Rev. Anal. Chem.* **2018**, *11* (1), 375−395.
(17) Becke, T. D.; Ness, S.; Gurster, R.; Schilling, A. F.; di Guilmi, A. M.; Sudhop, S.; Hilleringmann, M.; Clausen-Schaumann, H. Single Molecule Force Spectroscopy Reveals Two-Domain Binding Mode of Pilus-1 Tip Protein RrgA of Streptococcus pneumoniae to Fibronectin. *ACS Nano* **2018**, *12* (1), 549−558.
(18) Oh, Y. J.; Koehler, M.; Lee, Y.; Mishra, S.; Park, J. W.; Hinterdorfer, P. Ultra-Sensitive and Label-Free Probing of Binding Affinity Using Recognition Imaging. *Nano Lett.* **2019**, *19* (1), 612−617.
(19) Yu, H.; Siewny, M. G. W.; Edwards, D. T.; Sanders, A. W.; Perkins, T. T. Hidden dynamics in the unfolding of individual bacteriorhodopsin proteins. *Science* **2017**, *355* (6328), 945−950.
(20) Lenton, S.; Rhys, N. H.; Towey, J. J.; Soper, A. K.; Dougan, L. Highly compressed water structure observed in a perchlorate aqueous solution. *Nat. Commun.* **2017**, DOI: 10.1038/s41467-017-01039-9.
(21) Giganti, D.; Yan, K.; Badilla, C. L.; Fernandez, J. M.; Alegre-Cebollada, J. Disulfide isomerization reactions in titin immunoglobulin domains enable a mode of protein elasticity. *Nat. Commun.* **2018**, *9* (1), 185.
(22) Zakeri, B.; Fierer, J. O.; Celik, E.; Chittock, E. C.; Schwarz-Linek, U.; Moy, V. T.; Howarth, M. Peptide tag forming a rapid covalent bond to a protein, through engineering a bacterial adhesin. *Proc. Natl. Acad. Sci. U. S. A.* **2012**, *109* (12), E690−E697.
(23) Takahashi, H.; Rico, F.; Chipot, C.; Scheuring, S. alpha-Helix Unwinding as Force Buffer in Spectrins. *ACS Nano* **2018**, *12* (3), 2719−2727.
(24) Rico, F.; Gonzalez, L.; Casuso, I.; Puig-Vidal, M.; Scheuring, S. High-Speed Force Spectroscopy Unfolds Titin at the Velocity of Molecular Dynamics Simulations. *Science* **2013**, *342* (6159), 741−743.
(25) Valbuena, A.; Oroz, J.; Hervás, R.; Vera, A. M.; Rodríguez, D.; Menéndez, M.; Sulkowska, J. I.; Cieplak, M.; Carrión-Vázquez, M. On the remarkable mechanostability of scaffoldins and the mechanical clamp motif. *Proc. Natl. Acad. Sci. U. S. A.* **2009**, *106* (33), 13791−13796.
(26) Huang, W.; Wu, X.; Gao, X.; Yu, Y.; Lei, H.; Zhu, Z.; Shi, Y.; Chen, Y.; Qin, M.; Wang, W.; Cao, Y. Maleimide−thiol adducts stabilized through stretching. *Nat. Chem.* **2019**, *11* (4), 310−319.
(27) Xu, X. G.; Gilburd, L.; Bando, Y.; Golberg, D.; Walker, G. C. Defects and Deformation of Boron Nitride Nanotubes Studied by Joint Nanoscale Mechanical and Infrared Near-Field Microscopy. *J. Phys. Chem. C* **2016**, *120* (3), 1945−1951.
(28) Lei, H.; Guo, Y. B.; Hu, X. D.; Hu, C. G.; Hu, X. T.; Li, H. B. Reversible Unfolding and Folding of the Metalloprotein Ferredoxin Revealed by Single-Molecule Atomic Force Microscopy. *J. Am. Chem. Soc.* **2017**, *139* (4), 1538−1544.
(29) Li, H.; Zheng, P. Single molecule force spectroscopy: a new tool for bioinorganic chemistry. *Curr. Opin. Chem. Biol.* **2018**, *43*, 58−67.
(30) Beedle, A. E. M.; Lezamiz, A.; Stirnemann, G.; Garcia-Manyes, S. The mechanochemistry of copper reports on the directionality of unfolding in model cupredoxin proteins. *Nat. Commun.* **2015**, *6*, 7894.
(31) Xue, Y.; Li, X.; Li, H.; Zhang, W. Quantifying thiol−gold interactions towards the efficient strength control. *Nat. Commun.* **2014**, *5*, 4348.
(32) Ott, W.; Jobst, M. A.; Schoeler, C.; Gaub, H. E.; Nash, M. A. Single-molecule force spectroscopy on polyproteins and receptor−ligand complexes: The current toolbox. *J. Struct. Biol.* **2017**, *197* (1), 3−12.
(33) Yeh, A. P.; Hu, Y.; Jenney, F. E.; Adams, M. W. W.; Rees, D. C. Structures of the Superoxide Reductase from Pyrococcus furiosus in the Oxidized and Reduced States. *Biochemistry* **2000**, *39* (10), 2499−2508.
(34) Clay, M. D.; Cosper, C. A.; Jenney, F. E.; Adams, M. W. W.; Johnson, M. K. Nitric oxide binding at the mononuclear active site of reduced Pyrococcus furiosus superoxide reductase. *Proc. Natl. Acad. Sci. U. S. A.* **2003**, *100* (7), 3796−3801.
(35) Clay, M. D.; Jenney, F. E.; Noh, H. J.; Hagedoorn, P. L.; Adams, M. W. W.; Johnson, M. K. Resonance Raman Characterization of the Mononuclear Iron Active-Site Vibrations and Putative Electron Transport Pathways in Pyrococcus furiosus Superoxide Reductase. *Biochemistry* **2002**, *41* (31), 9833−9841.
(36) Deng, Y.; Wu, T.; Wang, M.; Shi, S.; Yuan, G.; Li, X.; Chong, H.; Wu, B.; Zheng, P. Enzymatic biosynthesis and immobilization of polyprotein verified at the single-molecule level. *Nat. Commun.* **2019**, *10* (1), 2775.
(37) Yang, R.; Wong, Y. H.; Nguyen, G. K. T.; Tam, J. P.; Lescar, J.; Wu, B. Engineering a Catalytically Efficient Recombinant Protein Ligase. *J. Am. Chem. Soc.* **2017**, *139* (15), 5351−5358.
(38) Ott, W.; Jobst, M. A.; Bauer, M. S.; Durner, E.; Milles, L. F.; Nash, M. A.; Gaub, H. E. Elastin-like Polypeptide Linkers for Single-Molecule Force Spectroscopy. *ACS Nano* **2017**, *11* (6), 6346−6354.
(39) Durner, E.; Ott, W.; Nash, M. A.; Gaub, H. E. Post-Translational Sortase-Mediated Attachment of High-Strength Force Spectroscopy Handles. *Acs Omega* **2017**, *2* (6), 3064−3069.
(40) Stahl, S. W.; Nash, M. A.; Fried, D. B.; Slutzki, M.; Barak, Y.; Bayer, E. A.; Gaub, H. E. Single-molecule dissection of the high-affinity cohesin−dockerin complex. *Proc. Natl. Acad. Sci. U. S. A.* **2012**, *109* (50), 20431−20436.
(41) Marko, J. F.; Siggia, E. D. Stretching DNA. *Macromolecules* **1995**, *28* (26), 8759−8770.
(42) Sharma, D.; Perisic, O.; Peng, Q.; Cao, Y.; Lam, C.; Lu, H.; Li, H. Single-molecule force spectroscopy reveals a mechanically stable protein fold and the rational tuning of its mechanical stability. *Proc. Natl. Acad. Sci. U. S. A.* **2007**, *104* (22), 9278−83.
(43) Hoffmann, T.; Tych, K. M.; Hughes, M. L.; Brockwell, D. J.; Dougan, L. Towards design principles for determining the mechanical stability of proteins. *Phys. Chem. Chem. Phys.* **2013**, *15* (38), 15767−15780.
(44) Scholl, Z. N.; Marszalek, P. E. AFM-Based Single-Molecule Force Spectroscopy of Proteins. *Methods Mol. Biol.* **2018**, *1814*, 35−47.
(45) Dietz, H.; Rief, M. Exploring the energy landscape of GFP by single-molecule mechanical experiments. *Proc. Natl. Acad. Sci. U. S. A.* **2004**, *101* (46), 16192−16197.
(46) Liu, Y.; Huang, Z.; Tan, X.; Wang, Z.; Zhang, X. Cucurbit[8]uril-based supramolecular polymers: promoting supramolecular polymerization by metal-coordination. *Chem. Commun.* **2013**, *49* (51), 5766−5768.
(47) Zheng, P.; Li, H. Highly Covalent Ferric-thiolate Bonds Exhibit Surprisingly Low Mechanical Stability. *J. Am. Chem. Soc.* **2011**, *133* (17), 6791−8.
(48) Perales-Calvo, J.; Lezamiz, A.; Garcia-Manyes, S. The Mechanochemistry of a Structural Zinc Finger. *J. Phys. Chem. Lett.* **2015**, *6* (17), 3335−3340.
(49) Wei, W.; Sun, Y.; Zhu, M.; Liu, X.; Sun, P.; Wang, F.; Gui, Q.; Meng, W.; Cao, Y.; Zhao, J. Structural Insights and the Surprisingly Low Mechanical Stability of the Au−S Bond in the Gold-Specific Protein GolB. *J. Am. Chem. Soc.* **2015**, *137* (49), 15358−15361.
(50) Moura, I.; Teixeira, M.; Moura, J. J. G.; LeGall, J. Spectroscopic studies of cobalt and nickel substituted rubredoxin and desulforedoxin. *J. Inorg. Biochem.* **1991**, *44* (2), 127−139.
(51) Becke, T. D.; Ness, S.; Sudhop, S.; Gaub, H. E.; Hilleringmann, M.; Schilling, A. F.; Clausen-Schaumann, H. Covalent Immobilization of Proteins for the Single Molecule Force Spectroscopy. *J. Visualized Exp.* **2018**, *138*, No. e58167.

DOI: 10.1021/acs.jpclett.9b01573
J. Phys. Chem. Lett. 2019, 10, 5428−5433